Paper C

CO_2-water-rock interactions – ACCRETE simulations of geological storage of CO_2.

Hellevang, H.
Kvamme, B.

Submitted to *Applied Geochemistry*

CO_2-water-rock interactions - ACCRETE simulations of geological storage of CO_2

H. Hellevang *, and B. Kvamme

Department of Physics and Technology, University of Bergen, Allégaten 55, N-5007 Bergen, Norway

Abstract

Increasing atmospheric concentrations of greenhouse gases are suspected of causing a gradual warming of the Earths surface, and possibly lead to disastrous changes in the global climate. Because carbon dioxide (CO_2) is a significant greenhouse gas, storage in saline aquifers has been suggested as one possible approach to reduce emissions of CO_2 to the atmosphere. In this study we focus on the CO_2-water-rock interactions which occur as a result of CO_2 injection into saline aquifers. Two different mineralogies that interact with a typical saline groundwater are simulated to show the sensitivity of permanent CO_2 storage on initial mineralogy, temperature and pressure. Simulations are performed using the geochemistry code ACCRETE, which has been developed to simulate long-term interactions between CO_2, aqueous solutions and minerals.

1. Introduction

Combustion of fossil fuel releases large quantities of carbon to the atmosphere. It is a grown concern that anthropogenic carbon emissions may have a significant impact on the climate through the greenhouse effect. Since CO_2 is believed to be a major contributor, different strategies of how to reduce emissions have been suggested. Some options that seem promising are underground storage in saline aquifers, storage in abandoned oil-, and gas fields and storage in deep unminable coal fields. CO_2 might also be used as an agent to enhance the recovery of hydrocarbon from producing oil and gas fields.

1.1. Geological storage of CO_2

Geological storage of CO_2 is injection of CO_2 into subsurface geological reservoirs. There are three main options for subsurface storage of CO_2: (1) storage in saline aquifers; (2) storage into existing oil and gas fields; and (3) storage into unminable coal seams (Baines and Worden, 2004). A comprehensive introduction to geological storage is given by Bouchard and Delaytermoz (2004). Several CO_2 storage projects are at present active or planned to start in the near future. The Sleipner injection site in the North Sea was the first industrial scale injection site. (Korbøl and Kaddour, 1995; Zweigel *et al.,* 2001; Torp and Gale, 2004). This site is still operational and is planned to inject for 20 years. Sites like Snøhvit (Northern Norway; Maldal and Tappel, 2004) and In Salah (Algerie; Riddiford et al., 2004) are shortly to follow. The annual combined reduction from the Sleipner and Snøhvit injection sites are estimated to 1.7 million tonnes. Once CO_2 is injected it starts to dissolve into the formation water and any excess gas or fluid phase will, due to its lower density, migrate towards the top of the formation. This excess CO_2 migration is of major importance on the short-term safety of the injection site. The dissolved CO_2 reacts with the water to form carbonic acid and lower the pH. This in turn makes the water reactive with respect to the minerals present in the reservoir. Dissolution of primary minerals leads to formation of new secondary minerals such as solid carbonates. Once formed these carbonates may contribute to a safe long-term storage of CO_2.

Since most mineral reactions are slow at reservoir conditions (some silicate grains may need thousands of years before disintegrating, Lasaga, 1998), the direct value of experimental work on the CO_2-water-rock interactions is limited and can only provide a glimpse into the qualitative and quantitative nature of the reactions. To gain information on the long-term fate of the CO_2 i.e., thousands of years, numerical codes that integrate results from multiple geochemical experiments have to be used.

The project "Long Term storage of CO_2 in aquifers" was initiated in 2003. The main focus of this project is long term (10000 years) and corresponding long range migrations of CO_2, its corresponding dissociated ions and ions from dissolved minerals that follow the flow in the reservoir. These ions may precipitate into other minerals in regions of the

* Corresponding author. Tel.: +47 5558 2878; Fax: +47 5558 9440
E-mail address: helgeh@ift.uib.no (H. Hellevang).

Submitted to Applied Geochemistry 10 November 2005

reservoir where pH is different and favorable for mineralisation. For this purpose we have enxtended the reservoir simulation code Athena to include geochemical reactions. The aim of this paper is to present the ACCRETE geochemistry code and to show results from batch simulations that are quantitatively comparable with published batch and reactive transport simulations.

1.2. ACCRETE, an Athena batch geochemistry module

ACCRETE is a F77 batch geochemistry code and is an acronym for **A**thena **C**arbon **C**apture and sto**R**age geoch**E**mis**T**ry modul**E**. The development of the code was initiated as the in-house Athena multiphase 3D flow research code, based on a secondary oil migration model, was expanded to cover geological storage of CO_2. ACCRETE is called as an external module for each Athena timestep and updates the geochemistry according to directives given by Athena. ACCRETE can also be run as a stand-alone batch geochemistry solver as in the case of this report. The present ACCRETE version (ACCRETEbatch v 1.0) simulates interactions between 16 mineral phases, 13 aqueous solutes, H_2O as a solvent, and CO_2 as a separate gaseous or supercritical phase.

Table 1
Ion-specific parameters used in the Truesdell-Jones model for estimations of activity coefficients for charged species.

Charged ion	a_i(Å)	b_i(L/mol)
Na^+	4.32	0.06
K^+	3.71	0.01
H^+	4.78	0.24
Mg^{2+}	5.46	0.22
Fe^{2+}	5.08	0.16
Ca^{2+}	4.86	0.15
Al^{3+}	6.65	0.19
Cl^-	3.71	0.01
OH^-	10.65	0.21
HCO_3^-	5.4	0
CO_3^{2-}	5.4	0

2. Methods

2.1. Thermodynamic calculations

The standard state adopted in this study is that of unit activity for pure minerals and H_2O at any temperature and pressure. For aqueous species other than H_2O, the standard state is unit activity of species in a hypothetical 1 molal solution referenced to infinite dilution at any temperature and pressure. For gases, the standard state is for unit fugacity of a hypothetical ideal gas at 1 bar pressure. Thermodynamic data are calculated with the SUPCRT92 program (Johnson et al., 1992) using the dprons96.dat database. Equilibrium constants for mineral reactions and speciation are calculated from standard state Gibbs free energy of formation ΔG_f^0 of the constituent components according to:

$$\ln\left(K^0\right) = -\frac{\Delta G_r^0}{RT}, \tag{1}$$

where R is the gas constant (8.3145 Joules/mol K), and T is absolute temperature, and the free energy of each reaction is calculated according to:

$$\Delta G_r^0 = \sum_p \Delta G_{f,p}^0 - \sum_r \Delta G_{f,r}^0 \,. \tag{2}$$

The temperature dependence of the equilibrium constants is given by:

$$\begin{aligned}
\ln\left(\frac{K^T}{K^0}\right) &= -\int_{T^0}^{T} \frac{\Delta H_r(T,P)}{R} d\left(\frac{1}{T}\right) \\
&= -\int_{T^0}^{T} \frac{\left\{\Delta H_r^0\left(T^0,P^0\right) + \int_{T^0}^{T} \Delta C_{P,r}\left(\theta,P^0\right) d\theta\right\}}{R}, \\
&\quad \frac{+\int_{P^0}^{P}\left[\Delta v_r - \Delta\left\langle T\left(\frac{\partial v}{\partial T}\right)_P\right\rangle_r\right] dP\Big\}}{} d\left(\frac{1}{T}\right) \\
&\approx -\frac{\Delta H_r^0}{R}\left(\frac{1}{T} - \frac{1}{T^0}\right)
\end{aligned} \tag{3}$$

where ΔC_{P_r} is difference in the specific heat capacity over the reaction and the latter term in the denominator contains the molar volume change, and the temperature derivative of the volume change over the reaction. Since the reactions are in liquid phase the volumetric effects on the enthalpy is small since volumes as well as temperature derivatives of volumes are small. The difference in specific heat capacities across the reaction is more reaction individual but in many cases the effect is negligible relative to other sources of errors. Neglecting the temperature dependence gives the Van'T Hoff expression (equation 3) as an approximation, which is also used in this work.

Non-idealities of charged dissolves aqueous species is solved according to the Truesdell-Jones activity model (Truesdell and Jones, 1974), valid for up to 2M NaCl dominated solutions:

$$\log \gamma_i = -\frac{A(T) z^2 \sqrt{I}}{1 + a_i B(T)\sqrt{I}} + b_i I \,, \tag{4}$$

Table 2
Coefficients a_{ij} for expression (5).

a_{11}	-3.3803410340x10^{-21}	a_{31}	-1.7796306552x10^{-15}	a_{51}	-3.2360510372x10^{-11}
a_{12}	5.5639792653x10^{-18}	a_{32}	2.9410588041x10^{-12}	a_{52}	5.3848036621x10^{-8}
a_{13}	-3.6439136441x10^{-15}	a_{33}	-1.9344534434x10^{-9}	a_{53}	-3.5679891752x10^{-5}
a_{14}	1.1862732957x10^{-12}	a_{34}	6.3266787924x10^{-7}	a_{54}	1.1761627764x10^{-2}
a_{15}	-1.9185324583x10^{-10}	a_{35}	-1.0282355457x10^{-4}	a_{55}	-1.9276764612
a_{16}	1.2322834905x10^{-8}	a_{36}	6.6388938521x10^{-3}	a_{56}	1.2556700906x10^{2}
a_{21}	4.0073137678x10^{-18}	a_{41}	3.6185059951x10^{-13}	a_{61}	9.3398080811x10^{-10}
a_{22}	-6.6076811370x10^{-15}	a_{42}	-5.9976115054x10^{-10}	a_{62}	-1.5620468551x10^{-6}
a_{23}	4.3356784554x10^{-12}	a_{43}	3.9572927542x10^{-7}	a_{63}	1.0407129649x10^{-3}
a_{24}	-1.4143495997x10^{-9}	a_{44}	-1.2985952833x10^{-4}	a_{64}	-3.451211675089x10^{-1}
a_{25}	2.2923655509x10^{-7}	a_{45}	2.1180695763x10^{-2}	a_{65}	5.6936914820x10^{1}
a_{26}	-1.4758025981x10^{-5}	a_{46}	-1.3726958393	a_{66}	-3.7351399850x10^{3}

where A and B are Debue-Huckel parameters, z is charge, I is ionic strength, and a_i and b_i are temperature dependent model parameters tabulated in table 1. The fugacity coefficient of CO_2 is calculated according to the SRK equation of state (Soave, 1972) according to:

$$\begin{aligned}\phi = &\left(a_{11}T^5 + a_{12}T^4 + a_{13}T^3 + a_{14}T^2 + a_{15}T + a_{16}\right)P^5 \\ &+ \left(a_{21}T^5 + ... + a_{26}\right)P^4 + ... + \left(a_{61}T^5 + ... + a_{66}\right)\end{aligned}, \quad (5)$$

where coefficients a_{ij} are listed in table 2.

2.2. *Density of the aqueous solution*

The density of H2O is calculated as a function of temperature, pressure and dissolved salts according to the algorithm from Batzle and Wang (1992):

$$\begin{aligned}\rho_w^s = &\rho_w^p(T,P) + S\{a + bS + cP - dPS \\ &+ T\left(e + fT - gS - hP + iPS\right)\}\end{aligned}, \quad (6)$$

where S is mass fraction NaCl, P is pressure (Mpa) and T is temperature (°C). Superscripts s and p denotes salt and pure water respectively. The coefficients a to r in expressions (6) and (7) is given in Batzle and Wang (1992). The density of pure water is calculated according to:

$$\begin{aligned}\rho_w^p(T,P) = &1 + jT - kT^2 + lT^3 \\ &+ P\left(m - nT + oT^2 - pT^3 - qP - rTP\right)\end{aligned}, \quad (7)$$

whereas the effect of dissolved CO_2 on density is calculated as a function of T and P according to Garcia (2001):

$$\rho_w = \rho_w^s + c_{CO_2}\left\{M_{CO_2} - \left(\bar{v}_{CO_2}\rho_w^s\right)\right\}, \quad (8)$$

where c_{CO2} is CO_2 concentration (moles CO_2 per m^3 solution), and $\bar{v}$ is the apparent molar volume of dissolved CO_2. This expression was originally used for the CO_2 effect on the density of freshwater, but should also provide an acceptable estimate for saline solutions.

2.3. *Chemical speciation*

The demands for a satisfactorily solved system is that the solution is mass balanced and charge neutral, and that equilibrium considerations are satisfied. The charge neutrality is achieved by defining the moles of H^+ as the sum of the charges of all N other charged species in the water phase.

$$\boldsymbol{a}_{H^+} = \gamma_{H^+} m_{H^+} = -\gamma_{H^+} \sum_{i=1}^{N} m_i z_i \,, \quad (9)$$

where $\boldsymbol{a}$ and γ denotes activity and activity coefficient (l/mol) of H^+ respectively.

The next step is to check if the total amount of dissolved carbon is greater or equal to the bubblepoint molefraction for the aqueous solution. The bubblepoint molefraction of CO_2 is calculated according to:

$$x_{CO_2}^b = \frac{P\phi}{K_H}\exp\left\{\frac{\bar{v}^\infty}{RT}(1-P)\right\}, \quad (10)$$

where ϕ is the fugacity coefficient of CO_2 at T and P, K_H is Henrys Law coefficient for CO_2 at T and a given salinity (ppm NaCl), and $\bar{v}^\infty$ is the infinite dilution partial molar volume of CO_2. An analytical expression for the Henrys Law coefficient as a function of T and S is used based on experimental data by Zheng et al. (1997). The Henrys law coefficient is corrected for pressure by a Poynting correction term. The carbon speciation is constrained

* Corresponding author. Tel.: +47 5558 2878; Fax: +47 5558 9440
E-mail address: helgeh@ift.uib.no (H. Hellevang).

by equation (9), the bubblepoint mole fraction of dissolved CO_2, and by equilibrium expressions (11) to (13):

$$\boldsymbol{a}_{H^+} = \frac{K_1 \boldsymbol{a}_{CO_{2,aq}}}{\boldsymbol{a}_{HCO_3}}, \quad (11)$$

$$\boldsymbol{a}_{OH^-} = \frac{K_w}{\boldsymbol{a}_{H^+}}, \quad (12)$$

$$\boldsymbol{a}_{CO_3^{2-}} = \frac{K_2 \boldsymbol{a}_{HCO_3^-}}{\boldsymbol{a}_{H^+}}, \quad (13)$$

These equations are solved by an iterative approach until the difference between $\boldsymbol{a}_{H+}$ in equations 9 and 11 is less than 10^{-10} (this requires usually less than 6 or 7 iterations).

2.4. Solving mineral reactions

The next step after computing the initial solution is to solve the mineral reactions. The magnitude of the reactions, except for calcite that is assumed in instant equilibrium with the solution, is constrained by the kinetics given by:

$$r_i = k_i S_i \left\{ e^{f(x1,x2,\ldots,x14)} - 1 \right\}, \quad (14)$$

where k and S are kinetic constant (mol/m^{2}s) at temperature T and reactive surface for the reactions respectively, and $f(x1, x2, ..., x14)$ describes the distance from equilibrium as a function of the aqueous components x_1 to x_{14}, expressed as the difference in free energy between equilibrium and the actual solution. The reactive surface area is for dissolution regarded as proportional to the mass of the phase present. The reactive surface areas for individual minerals are equivalent to the specific reactive surface areas used in Johnson et al. (2001). Reactive surface area for precipitation is assumed equivalent to a fraction of the total surface area present in the reservoir (0.01 in this study). The changes in the aqueous components that accompany the mineral reactions can be expressed by:

$$\mathbf{X} = \Delta t \cdot \mathbf{RV}, \quad (15)$$

where $\mathbf{R}$ is an 1×16 matrix that contains rates for the mineral reactions calculated by expression (16), $\mathbf{V}$ is a 16×15 matrix that contains the number of each aqueous component in each reaction, and Δt is the size of the timestep. The latter value is reduced in size if the mineral reactions result in negative concentrations for any of the aqueous components. Once an appropriate timestep is found, the resulting aqueous solution is modified to satisfy carbon- and charge balance. The mineral reactions are solved once the total time for all subtimesteps equals the predefined global timestep. Calcite is solved as an equilibrium reaction rather than constrained by kinetics since the calcite reaction is assumed to be several order of magnitude faster than the other reactions (table 4), and is usually expected to reach a close to equilibrium state after only a few hours or days. This assumption is justified by experimental work on reservoir sand at reservoir conditions (e.g., Czernichowski-Lauriol et al., 2002).

Table 3
Initial aqueous chemistry for the simulations.

Component	X_i (mol/mol)
pH	**7.1**
Ca^{2+}	$1.33\text{x}10^{-4}$
$CO_{2,aq}$	0
HCO_3^-	$4.14\text{x}10^{-5}$
Na^+	$8.07\text{x}10^{-3}$
Cl^-	$9.30\text{x}10^{-3}$
Al^{3+}	$2.32\text{x}10^{-10}$
CO_3^{2-}	0
Mg^{2+}	$3.24\text{x}10^{-4}$
$SiO_{2,aq}$	$2.97\text{x}10^{-4}$
K^+	$9.50\text{x}10^{-5}$
Fe^{2+}	0

3. Simulations of geological storage using the ACCRETE simulator

Two different systems that differ both in mineralogy and physical conditions are simulated. Both simulations cover 10.000 years of interactions between minerals, and an aqueous solution and a supercritical CO_2 phase that fills the pore space. The first system is the Utsira Sand at the Sleipner injection site, which is well described both with respect to geochemistry and its physical conditions (e.g., Zweigel et al., 2001; Chadwick et al., 2004). The Utsira Formation has also been simulated by other researchers (e.g., Johnson et al., 2001; 2004; Gaus et al., 2003) and is useful for comparisons between ACCRETE and other numerical tools. The Utsira sand used in this study is a mixture of 5% clay and 95% sand adopted from data in Johnson et al. (2001). This is done to simulate a batch of the Utsira sand which is interpreted to consist of sands separated by clay horizons (e.g., Zweigel et al., 2001). The second system, Glauconitic sand, is adopted from Xu et al. (2004), who used the system for 100.000 years batch simulations of CO_2 injection. This Glauconitic sand is a proxy for a glauconitic sandstone aquifer from the Alberta Sedimentary Basin (see Gunter et al., 1997). Table 4 summarises the simulation data for the two systems. An initial aqueous chemistry, believed to resemble Utsira Pore water, adopted from Johnson et al. (2001), is used for both systems (see Table 3). This is done to illustrate the isolated effect of different mineral assemblages and physical conditions on the injected CO_2.

Table 4.
Initial mineral volume fractions and kinetic data for Utsira sand and glauconitic sand respectively.

Mineral	x^{Utsira}	$x^{glauconitic}$	k_{25} (mol/m^{2}s)	Ea (kJ/mol)	S (cm^2/cm^3)
Calcite	0.0285	0.013	Equilibrium	62.8	$1.00x10^{2}$
Magnesite	0	0.005	$1.00x10^{-9}$	62.8	$1.00x10^{2}$
Siderite	0	0.01	$1.00x10^{-9}$	62.8	$1.00x10^{2}$
Dawsonite	0	0	$3.06x10^{-11}$	62.8	$2.44x10^{4}$
Albite	0.03	0	$1.00x10^{-12}$	80.3	$8.75x10^{2}$
Microcline	0.038	0.02	$1.78x10^{-13}$	51.7	$1.11x10^{3}$
Quartz	0.496	0.72	$1.04x10^{-14}$	87.7	$5.74x10^{2}$
Chalcedony	0	0	$3.45x10^{-13}$	87.7	$1.25x10^{4}$
Kaolinite	0	0.02	$4.00x10^{-13}$	29.0	$1.25x10^{4}$
Clinochlore-14A	0.003	0	$3.00x10^{-13}$	88.0	$1.25x10^{4}$
Daphnite-14A	0	0	$3.00x10^{-13}$	88.0	1.25x104
Muscovite	0.04025	0	$1.00x10^{-13}$	22.0	$1.25x10^{4}$
Phlogopite	0.01425	0.04	$4.00x10^{-13}$	29.0	$1.25x10^{4}$
Annite	0	0.04	$4.00x10^{-13}$	29.0	$1.25x10^{4}$
Labradorite	0	0.01	$2.04x10^{-10}$	42.1	$8.06x10^{2}$
Gibbsite	0	0	$3.16x10^{-12}$	53.0	$8.66x10^{3}$
Porosity	0.35	0.122			

Because of differences between the mineral assemblages in ACCRETE and the compiled assemblages from Xu et al. (2004) some modifications were done. For example is glauconite and illite in the glauconitic sand approximated by a 50/50 mixture of phlogopite and annite in ACCRETE, and oligoclase is approximated by labradorite (see details in table footnotes). Kinetic data for the mineral reactions are, with some exceptions, adopted from a compilation in Johnson et al. (2001). The exceptions are dawsonite (Hellevang et al., 2005), gibbsite (Ganor et al., 2005), labradorite (Carroll and Knauss, 2005). Annite is assumed to have same kinetic properties as phlogopite (Table 4).

3.1. Results

Three principal steps that together lead to permanent transformation of CO_2 into solid carbonates are: (1) Dissolution of CO_2 into aqueous solutions; (2) dissolution of primary silicates that releases cations for the carbonates; and (3) precipitation of solid carbonates. The results from the ACCRETE simulations are presented in sections (3.1.1) to (3.1.3) in figures 1 to 3 to illustrate these three principal steps, whereas section (3.1.4) presents the temporal effect of the water-rock interaction on porosity for the two simulated systems.

3.1.1. Dissolution of CO_2

The solubility of CO_2 into the aqueous phase is of major importance for the reactivity of the system, mainly because of a significant drop in pH. The solubility is estimated in ACCRETE by expression (10) which provides the bubblepoint mole fraction of CO_2. The CO_2 that dissolves reacts with the water in the aqueous solution and form carbonic acid, and bicarbonte- and carbonate ions. The distribution of these species is strongly dependent on the pH. Fig. 1 shows the temporal evolution of the different carbon species and pH for Utsira- and glauconitic sand respectively. CO_2 as a separate phase occupy initially 20% of the available porespace for both systems. The initial amount of CO_2 in the glauconitic sand is approximately 1/3 of the Utsira sand since the porosity of the former is much smaller (0.112 versus 0.35; see table 4). The glauconitic sand is also different with a higher rock/water ratio, higher temperature, and a higher fraction reactive phyllosilicates. The above differences lead to a total consumption of the CO_2 phase in the glauconitic sand after less than 200 years, whereas a separate CO_2 phase is still present in the Utsira sand after 10.000 years. Followed by the consumption of the free CO_2 the aqueous CO_2 (CO_2,aq) drops as solid carbonates continues to precipitate. As presented in section 3.1.3 the consumption of the free CO_2 has pronounced effects on the stability of the early formed solid carbonates.

3.1.2. Major silicate reactions

Dissolution of primary silicates which increase the cation content of aqueous solutions and supersaturates carbonates is the primary driving mechanism for geological storage of CO_2. The nature of the carbonate precipitates is directly related to the silicates that dissolve.

* Corresponding author. Tel.: +47 5558 2878; Fax: +47 5558 9440
E-mail address: helgeh@ift.uib.no (H. Hellevang).

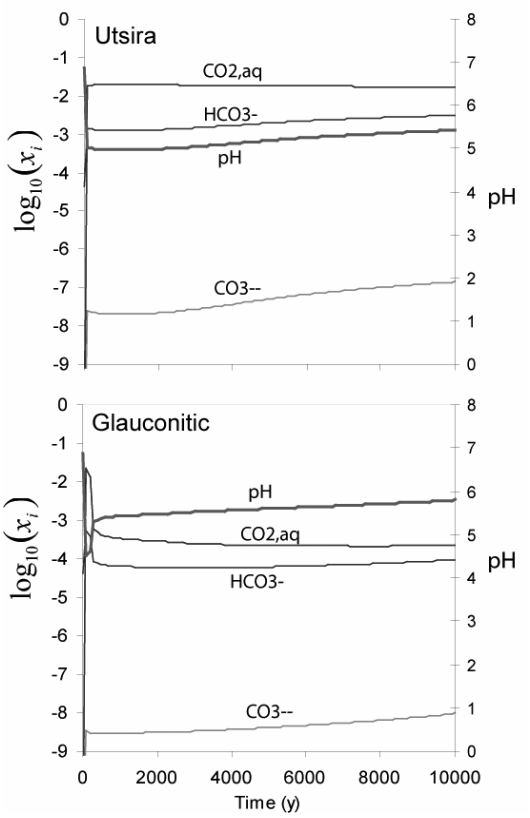

Fig. 1. Temporal evolution of carbonate species and pH for Utsira sand and glauconitic sand respectively.

The temporal evolution of silicates for Utsira sand and glauconitic sand, i.e. the relative change in volume fraction, is illustrated in Fig. 2. For each system only the major reactions have been included. Common for both systems is a massive dissolution of the phyllosilicate phlogopite that releases 3 moles of Mg^{2+} ions for each mole of mineral that dissolves. This leads to, as presented in the next section, large-scale precipitation of magnesite. In the Utsira sand, almost 100% (1.5 vol%) of the initial phlogopite dissolves, whereas the glauconitic sand still retains some phlogopite after 10.000 years. Other major dissolving silicates are clinochlore in the Utsira sand, that releases 5 moles of Mg^{2+} ions for each mole dissolved , and annite (3 Fe^{2+}), kaolinite, and labradorite (0.6 Ca^{2+}) in the glaconitic sand. The dissolution of the silicates also contribute with aluminum to the aqueous solution, which has been suggested could lead to dawsonite ($NaAl(OH)_2CO_3$) precipitation. Figure 2 shows however that the dissolution of some silicates are balanced by the precipitation of others like daphnite and muscovite. Not included in this figure is the (minor) precipitation of gibbsite ($Al(OH)_3$) that is instrumental in keeping a low aluminum concentration in the solutions. The next sections show that dawsonite is only a minor precipitating phase in these simulations.

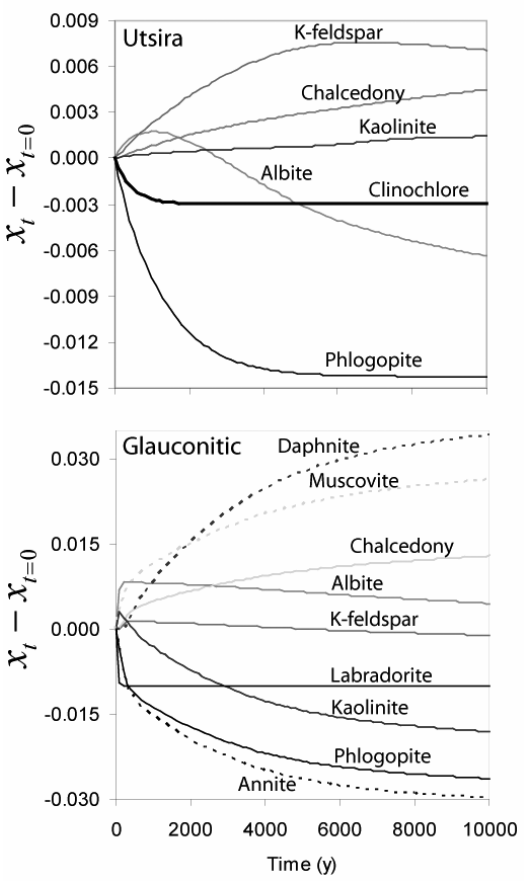

Fig. 2. Difference between initial volume fraction and volume fraction at time *t* for major silicate reactions for Utsira sand and glauconitic sand respectively.

3.1.3. Permanent storage in solid carbonates

Figure (3) shows the relative change in solid carbonates with time ($\Delta(V_i/V_{tot})$). The maximum possible storage is shown in the glauconitic sand where all 20 vol% of the CO_2 phase initial present in the pore space is consumed after less than 200 years. At this point the total stored carbon is 1.22 vol%. The formation of carbonates in the Utsira sand is significantly slower and 2.54 vol% of the CO_2 initial present in the pore space is still not consumed after 10.000 years. The maximum amount of carbon stored in the latter case is 1.01 vol%. ACCRETE provides four possible carbonates: magnesite, calcite, siderite, and dawsonite. The simulations suggest that magnesite and calcite is totally dominating in the Utsira sand, whereas siderite is dominating together with magnesite in the Glauconitic sand before the CO_2 phase is consumed and siderite is destabilised. Dawsonite is only forming a minor fraction of the total precipitated carbonates.

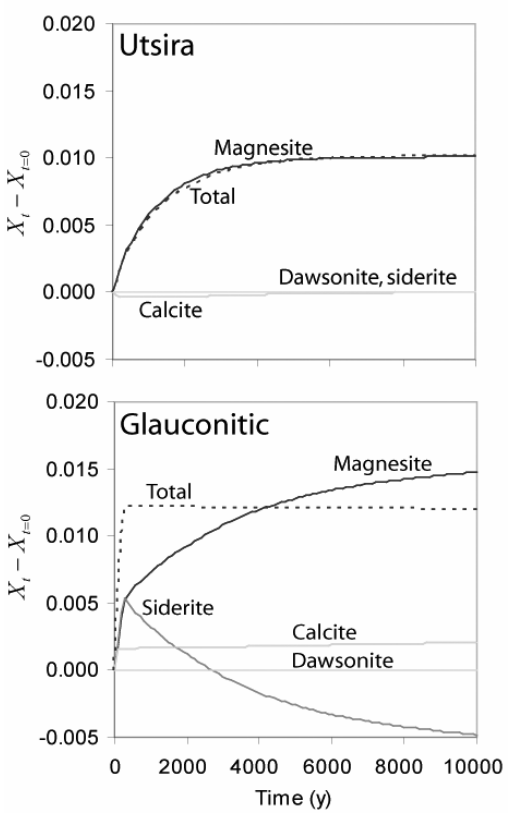

Fig. 3. Permanent storage of CO_2 as solid carbonates for Utsira sand and glauconitic sand respectively. Y-axis shows that difference between initial mineral volume fraction and volume fraction at time *t*.

3.1.4. Temporal evolution of porosity

Fig. 4 shows the relative change in porosity for Utsira sand and glauconitic sand respectively. The figure suggests that the precipitation of carbonates and secondary silicates only slightly affect the porosity. The reason for this is that dissolution of primary minerals that increases the porosity is accompanied with precipitation of other secondary silicates and carbonates that decrease the porosity. It is however a general decrease in porosity as the mass of carbon in CO_2 is transferred to the solid matrix. As indicated in Fig. 3 the glauconitic sand is more reactive, and this is also observed in the temporal evolution of the porosity. The maximum change for the glauconitic sand is seen after 10.000 years with a reduction from approximately 0.112 to 0.107.

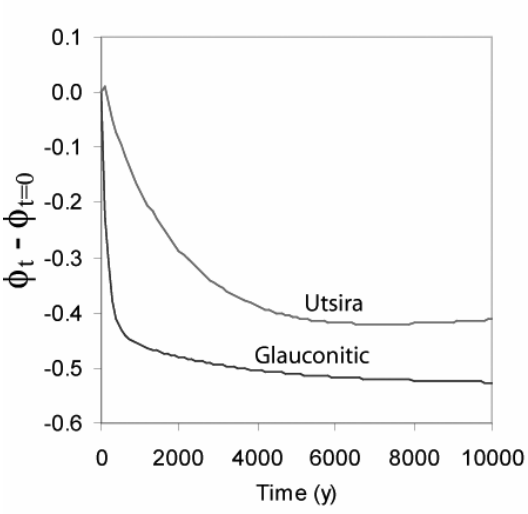

Fig. 4. Temporal evolution of porosity for Utsira sand and glauconitic sand respectively.

4. Discussion

4.1. Comparisons between ACCRETE simulations and published batch- and reactive transport simulations

The outcome of numerical simulations of CO_2 storage is largely dependent on the choice of mineral assemblages, thermodynamic data, and by kinetic parameters of mineral reactions. As seen in the previous section, different ACCRETE simulations with different mineralogies and physical conditions provide results that vary significantly with respect to both nature and magnitude of reactions. It is however some general properties that can be compared to published batch- and reactive transport simulations like: (1) dominant carbonates forming from the interactions; (2) dominant silicate reactions; (3) magnitude of the geological storage with time; and (4) changes in porosity. The ACCRETE simulations are compared to published simulations by Xu et al. (2004), White et al. (2003), and Knauss et al. (2005), hereby refereed to as XU04, WH03, and KN05 respectively. These simulations vary from 100 years reactive transport simulations (KN05), to 100.000 years batch simulations (XU04). Simulations by ACCRETE shows that calcite is the second most abundant phase in the glauconitic sand (Fig. 6) and calcite is also found as a dominating phase in all three published simulations. Magnesite on the other hand is not considered in the XU04 and WH03 simulations, and constitutes a minor carbonate phase in KN05. The most striking difference is however the low abundance of dawsonite precipitated in the ACCRETE simulations compared to the others. This can partly be explained by a much higher sodium concentration in KN05, which on a short timescale will result in enhanced precipitation of dawsonite.

The difference can also be explained by the use of labradorite ($Ca_{0.6}Na_{0.4}Al_{1.6}Si_{2.4}O_8$) in ACCRETE instead of oligoclase ($Ca_{0.2}Na_{0.8}Al_{1.2}Si_{2.8}O_8$) as used by XU04, and that a slower kinetic constant is used for dawsonite in ACCRETE. Silicate reactions that are observed in glauconitic sand in ACCRETE simulations are qualitatively similar to the glauconitic sandstone simulated in XU04. The observed dissolution of kaolinite, labradorite (oligoclase in XU04) and annite (glauconite in XU04), and precipitation of k-feldspar are common for both ACCRETE and XU04. Dissolution of labradorite (KN05) and anorthite (WH01) and precipitation of calcite is also comparable with ACCRETE. One major difference between ACCRETE and XU04 is illite that precipitates in XU04, whereas phlogopite used as a proxy in ACCRETE dissolves. Fig. 6 illustrates the amount of CO_2 stored as solid carbonates. The maximum amount found in the glauconitic sand was approximately 1.22 vol% after less than 200 years. By comparison, the glauconitic sand of XU04 stored approximately 1.2 vol% after 10.000 years, whereas KN04 rapidly formed 0.9 vol% after 5 years of injection. Thus, results from ACCRETE are somewhere between XU04 and the rapid formation in KN05. Because of differences in initial conditions and timeframe it is hard to make good quantitative comparisons.

Porosity is an important variable with respect to flow properties and is usually set proportional to the permeability through for example a Cozeny-Karman type of expression. It is therefore important to relate temporal changes in porosity to chemical reactions. Fig. 4 suggests that changes in porosity caused by CO_2 charged water interacts with the mineralogy is minor. These changes are comparable with the glauconitic sand in XU04 which also reports only minor changes.

4.2. Comparisons with natural analogues

Naturally occurring CO_2 deposits can be regarded as large-scale natural laboratories and they provide excellent opportunities to study long-term CO_2-water-rock interactions. Such natural deposits occur worldwide in a wide range of different sediments and rock types. Examples of such deposits are the Springerville-St. Johns CO_2 field in USA, the Ladbroke Grove and Katnook gas fields in Australia, as well as several natural analogues in Europe (Stevens et al., 2001).

The Springerville-St. Johns CO_2 field is one of several similar reservoirs developed in domed Mesozoic and Paleozoic sedimentary rocks of the Colorado Plateau and Southern Rocky Mountain region of the western U.S. (Moore et al., 2003). Detailed petrographic analyses are reported for well 22-1X from depths between 462 to 472 meters, that represented the only interval that showed clear evidence for interactions with CO_2 charged fluids (Moore et al., 2003). Major reactions observed in the reported interval are dissolution of authigenic cements, dissolution of detrial feldspar grains, and formation of dawsonite and kaolinite. Textural evidence suggests that early dolomite and hematite were followed by anyhydrite and calcite cements. Dawsonite and kaolinite is interpreted to be the latest phases, with kaolinite inferred to be the younger of the two. While dawsonite is limited to the interval between 462 and 472 meters, Kaolinite is a common mineral in core samples from all wells and generally comprises from 2 to 7 weight% of the rock.

The Ladbroke Grove and Katnook gas fields are located within the Penola Through of western Otway Basin (Watson et al., 2004). Recent volcanic activity (<1 Ma) lead to CO_2 migration into the Pretty Hill Formation, with CO_2 levels that range from 26 to 57 mol% in the Ladbroke Grove Field. The same formation in the Katnook Field less than 1 km away is charged with pure methane (Watson et al., 2004). The recent influx of CO_2 together with the difference in CO_2 levels makes these fields excellent as a natural laboratory for studying CO_2-water-rock interactions. The major reactant minerals interpreted to be in the formations prior to the CO_2 influx are feldspars, volcanic rock fragments, chlorite, and calcite. The feldspars are predominantly altered to sodium plagioclase, whereas the chlorite resulted from chloritisation of volcanic rock fragments. Both these alterations are interpreted to be prior to the influx of CO_2. Calcite occurs as a cementing phase in concretions up to 5 cm in size. The minerals in the Pretty Hill Formation in the Ladbroke Grove Gas field show extensive evidence of interactions with CO_2. The main mineral products are secondary quartz, kaolinite, and ferroan carbonates. The chlorite in Katnook is almost totally replaced by kaolinite. Calcite cements as found in Katnook is only present below the gas-water contact in the Ladbroke field.

Even if these two systems are different with respect to initial mineralogies, temperatures, length of interactions with CO_2, etc., some general qualitative similarities can be noted, and compared with the ACCRETE simulations. First, kaolinite is observed to form a major precipitate after dissolution of aluminosilicates in both natural systems. Precipitation of kaolinite as a reaction product of silicate dissolution is also observed in both simulations by ACCRETE as long as the aqueous phase is CO_2 saturated. Kaolinite is however dissolving once the CO_2 phase is consumed in the glauconitic case. The second similarity that is worth noting in the natural systems is dissolution of authigenic cements. In the Ladbroke gas field, calcite cement is only found below the gas-water contact. This compare to the initial fast dissolution of calcite in both simulated systems. The magnitude of the dissolution is however limited by the static batch approach. Other field observations like precipitation of Fe-carbonates and

dawsonite seems to be restricted to the individual mineralogies and chemistries of the natural systems.

4.3. How does the ACCRETE code perform?

4.3.1. CO_2 solubility in saline solutions

The solubility of CO_2 is of major importance for estimating the storage potential of a system. On short timescale (a few years) solubility trapping totally dominates over mineral trapping, and it is detrimental for the movement and retention of the supercritical or gaseous CO_2. Equation (10) as used here is a very simple model describing the solubility of CO_2 in saline solutions. In order to see how expression (10) performs, it is compared with the much more sophisticated algorithms by Duan and Sun (2003). They present rigorous algorithms for a large range in temperature, pressure and salinities, and compare results with a large number of experimental data, and shows that their model fits closely to the experimental data. Fig. 5 shows a quantitative comparison for a 1 molal NaCl solution between ACCRETE (equation (10)) and estimated data from Duan and Sun (2003) at different temperatures and pressures. The figure suggests that ACCRETE calculations is comparable at temperatures below 333K and for pressures up to 200 bar. At higher temperatures the solubility is underestimated, whereas the solubility is overestimated at high pressures. As a result of the contrary effect temperature and pressures has on the solubility, expression (10) provides good estimates for most reservoir settings even at high pressures and temperatures.

4.3.2. Mineral reactions

Section 4.1 shows that simulations of the Utsira sand and glauconitic sand are, to different degrees, qualitatively comparable with other numerical works and to natural analogues of CO_2 storage. Qualitative similarities with other numerical tools are expected since much of the kinetic- and thermodynamic framework is similar. Some important differences are however noted because of differences in primary minerals and possible secondary minerals. The choice of phyllosilicates and sometimes plagioclase composition (e.g., oligoclase in Xu et al., 2004) in different numerical studies is shown to be instrumental both with respect to the amount of CO_2 that is stored as solid carbonates, the nature of the precipitates, and how fast the CO_2 is converted. Since the current knowledge of kinetic- and thermodynamic stabilities of minerals to a large extent is limited to end-member compositions, these are used as proxies to the natural occurring varieties. Especially detailed knowledge of individual mineral reaction kinetics is lacking in the different numerical studies. For this reason one might expect significant deviations between simulations and natural systems. Thus, an increased effort should be directed to reduce the number of these master-unknowns. Comprehensive laboratory studies of phyllosilicates and carbonates will probably prove especially important in understanding long-term CO_2-water-rock interactions.

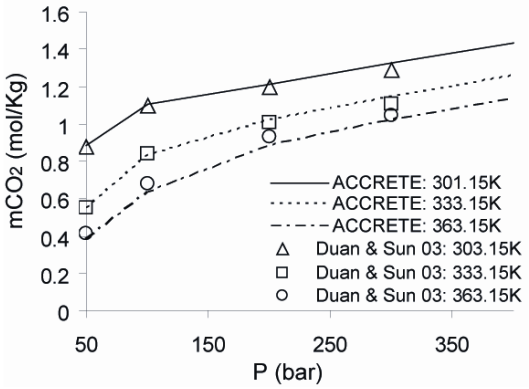

Fig. 5. Comparisons of solubilities of CO_2 in a 1 molal solution at different T and P between ACCRETE (this study) and Duan & Sun (Duan and Sun, 2003).

5. Concluding remarks

This study presents batch simulations of long-term (10.000 years) CO_2-water-rock interactions for two different mineralogies; Utsira sand, and glauconitic sand. The simulations shows a fast initial dissolution of CO_2 into the aqueous phase, before the CO_2 is gradually consumed and transferred into solid carbonates by the water-mineral interactions. Dissolution of primary silicates, primarily phlogopite, leads mainly to precipitation of the Mg-carbonate magnesite, whereas calcite constitutes the second most abundant carbonate product caused by dissolution of labradorite. The Fe-carbonate siderite is stable in the glauconitic sand system until the CO_2 phase is consumed and the aqueous carbonate concentration is lowered. The porosity shows only minor changes, but is seen to drop rapidly during the first years in the glauconitic sand before the CO_2 phase is consumed. Comparisons with numerical studies by Xu et al. (2004), White et al. (2003), and Knauss et al. (2005) shows both similarities and dissimilarities which are suggested stems principally from differences in the use of primary and secondary forming minerals. Comparisons with natural systems also show similarities with features of general character, like formation of kaolinite from aluminosilicate dissolution, and dissolution of authigenic cements. The nature of the carbonate precipitates are strongly system dependent. Limited databases, especially with respect to kinetic- and thermodynamic stabilities of phyllosilicates, constraint to some degree the confidence of simulations of long-term interactions between CO_2, waters, and minerals. This suggests that more work

should be concentrated on assemble thermodynamic and kinetic data for the mineral constituents of natural systems.

Acknowledgements

We thank Gunnar Fladmark and Sanjay Kumar for helpful discussions during the development of the ACCRETE geochemistry code. We would also like to thank Atle Svandal and Trygve Buanes for creative input in search for a more or less meaningful name for the ACCRETE code. The authors acknowledge Per Aagaard and Eric Oelkers for fruitful discussion regarding CO_2-water-rock interactions. The authors greatly acknowledge financial support from the Norwegian Research Council and Norsk Hydro.

References

Baines, S.J., Worden, R.H., 2004. Geological storage of carbon dioxide. In: Baines, S.J., and Worden, R.H. (eds), Geological Storage of Carbon Dioxide. Geological Society, London, Special Publications, 233, 1-6.

Batzle, M., Wang, Z., 1992. Seismic properties of pore fluids. Geophysics 57, 1396–1408.

Bouchard, R., Delaytermoz, A., 2004. Integrated path towards geological storage. Energy, 29, 1339-1346.

Carroll, S. A., Knauss, K. G., 2005. Dependence of labradorite dissolution kinetics on $CO_{2(aq)}$, Al_{aq}, and temperature. Chem. Geol. 217, 213–225.

Chadwick, R. A., Zweigel, P., Gregersen, U., Kirby, G. A., Holloway, S., Johannessen, P. N., 2004. Geological reservoir characterization of a CO_2 storage site: The utsira sand, sleipner, northern North Sea. Energy 29, 1371–1381.

Czernichowski-Lauriol, I., Rochelle, C. A., Brosse, E., Springer, N., Bateman, K., Kervevan, C., Pearce, J. M., and Sanjuan, B., 2002. Reactivity of injected CO_2 with the Utsira Sand reservoir at Sleipner**.** GHGT6, Kyoto, Japan, 1.-4.Okt.

Duan, Z., Sun, R., 2003. An improved model calculating CO_2 solubility in pure water and aqueous NaCl solutions from 273 to 533 K and from 0 to 2000 bar. Chem. Geol. 193, 257–271.

Ganor, J., Mogollon, J. L., Lasaga, A. C., 2005. Kinetics of gibbsite dissolution under low ionic strenth conditions. Geochim. Cosmochim. Acta 63 (11-12), 1635–1651.

Garcia, J. E., 2001. Density of aqueous solutions of CO_2. LBNL-49023, Lawrence Berkeley National Laboratory, Berkeley, California.

Gaus, I., Azarounal, M., Chernichowski-Lauriol, I., 2003. Reactive transport modeling of dissolved CO_2 in the cap rock base during CO_2 sequestration (Sleipner site, North Sea). In: Proc. 2nd. Nat. Conf. Carb. Seq., Alexandria, Va, May 5-8.

Hellevang, H., Aagaard, P., Oelkers, E. H., Kvamme, B., 2005. Can dawsonite permanently trap CO_2? Accepted for publication in Env. Sci. Tech.

Johnson, J. W., Nitao, J. J., Steefel, C. I., Knauss, K. G., 2001. Reactive transport modeling of geologic CO_2 sequestration in saline aquifers: the influence of intra-aquifer shales and the relative effectiveness of structural, solubility, and mineral trapping during prograde and retrograde sequestration. In: Proc. 1st. Nat. Conf. Carb. Seq., Washington, May 14-17.

Johnson, J. W., Oelkers, E. H., Helgeson, H. C., 1992. SUPCRT92: a software package for calculating the standard molal thermodynamic properties of minerals, gases, aqueous species, and reactions from 1 to 5000 bar and 0 to 1000°C. Comput. Geosci. 18 (7), 899–947.

Knauss, K. G., Johnson, J. W., Steefel, C. I., 2005. Evaluation of the impact of CO_2, co-contaminant gas, aqueous fluid and reservoir rock interactions on the geologic sequestration of CO_2. Chem. Geol. 217, 339–350.

Korbøl, R., Kaddour, A., 1995. Sleipner vest CO_2 disposal – Injection of removed CO_2 into the Utsira Formation. Energ. Convers. Manage., 36, 509-512.

Lasaga, A. C., 1998. Kinetic theory in earth sciences. Princeton University Press, New Jersey.

Maldal, T., Tappel, I. M., 2004. CO_2 underground storage for Snøhvit gas field development. Energy 29, 1403–1411.

Moore, J., Adams, M., Allis, R., Lutz, S., Rauzi, S., 2003. CO_2 mobility in natural reservoirs beneath the Colorado Plateau and southern Rocky Mountains: An example from the Springerville-St.johns field, Arizona and New Mexico. In: Proc. 2nd. Nat. Conf. Carb. Seq., Alexandria, Va, May 5-8.

Riddiford, F., Wright, I., Bishop, C., Espie, T., Tourqui, A., 2004. Monitoring geological storage the In Salah gas CO_2 storage project. GHGT7, Vancouver, Canada, 5.-9.Sept.

Soave, G., 1972. Equilibrium constants from a modified Redlich-Kwong equation of state. Chem. Eng. Sci. 27, 1197–1203.

Stevens, S. H., Pearce, J. M., Rigg, A. A. J., 2001. Natural analogues for geologic storage of CO_2: An integrated global research program. In: Proc. 1st. Nat. Conf. Carb. Seq., Washington, May 14-17.

Torp, T.A., Gale, J., 2004. Demonstrating Storage of CO_2 in Geological Reservoirs: The Sleipner and Sacs Projects. Energy, 29, 1361-1369.

Truesdell, A. H., Jones, B. F., 1974. WATEQ, a computer program for calculating chemical

equilibria of natural waters. J. Res., U.S. Geological Survey 2, 233–274.

Watson, M. N., Zwingmann, N., Lemon, N. M., 2004. The Ladbroke-Grove-Katnook carbon dioxide natural laboratory: A recent CO_2 accumulation in a lithic sandstone reservoir. Energy 29, 1457–1466.

White, S. P., Allis, R. G., Moore, J., Chidsey, T., Morgan, C., Gwynn, W., Adams, M., 2003. Injection of CO_2 into an unconfined aquifer located beneath the Colorado, Central Utah, USA. In: Proc. 2nd. Nat. Conf. Carb. Seq., Alexandria, VA, May 5-8.

Xu, T., Apps, J. A., Pruess, K., 2004. Numerical simulation of CO_2 disposal by mineral trapping in deep aquifers. Appl. Geochem. 19, 917–936.

Zheng, D. Q., Guo, T. M., Knapp, H., 1997. Experimental and modeling studies on the solubility of CO_2, $CHClF_2$, CHF_3, $C_2H_2F_4$ and $C_2H_4F_2$ in water and aqueous NaCl solutions under low pressures. Fluid Phase Equilibr. 129, 197–209.

Zweigel, P., Hamborg, M., Arts, R., Lothe, A., Sylta, Ø., Tømmerås, A., 2001. Results and experiences from the first industrial-scale underground CO_2 sequestration case (Sleipner field, North Sea). In: 2001 AAPG Annual Meeting, Denver, abstract volume (CD) 6p.